EURASIP Journal on Applied Signal Processing 2005:16, 2730–2738

Comparison of Antenna Array Systems Using OFDM for Software Radio via the SIBIC Model

Khoi D. Le

Department of Electrical Engineering, University of Nebraska-Lincoln, Lincoln, NE 68588, USA

School of Electrical and Computer Engineering, University of Oklahoma, Norman, OK 73019, USA
Email: khoi@ou.edu

Michael W. Hoffman

Department of Electrical Engineering, University of Nebraska-Lincoln, Lincoln, NE 68588, USA
Email: mhoffman1@unl.edu

Robert D. Palmer

School of Meteorology, University of Oklahoma, Norman, OK 73019, USA
Email: rpalmer@ou.edu

Received 31 January 2004; Revised 28 October 2004

This paper investigates the performance of two candidates for software radio WLAN, reconfigurable OFDM modulation and antenna diversity, in an indoor environment. The scenario considered is a 20 m × 10 m × 3 m room with two base units and one mobile unit. The two base units use omnidirectional antennas to transmit and the mobile unit uses either a single antenna with equalizer, a fixed beamformer with equalizer, or an adaptive beamformer with equalizer to receive. The modulation constellation of the data is QPSK and 16-QAM. The response of the channel at the mobile unit is simulated using a three-dimensional indoor WLAN propagation model that generates multipath components with realistic spatial and temporal correlation. An underlying assumption of the scenario is that existing antenna hardware is available and could be exploited if software processing resources are allocated. The results of the simulations indicate that schemes using more resources outperform simpler schemes in most cases. This implies that desired user performance could be used to dynamically assign software processing resources to the demands of a particular indoor WLAN channel if such resources are available.

Keywords and phrases: OFDM modulation, multipath channel, indoor radio stochastic channel model, wireless LAN.

1. INTRODUCTION

Widespread use of portable wireless systems demands maximum efficiency in the use of fundamental resources such as frequency bands or time slots. In addition, software radio applications provide the possibility for, and require the availability of, variable rates and quality of service for a large and diverse set of user needs. Extremely flexible modulation strategies such as those provided by orthogonal frequency division multiplexing (OFDM) [1] mesh nicely with both the wide range of user requirements and the necessity for a software radio to be relatively easy to control via simple changes in the system programming. A potential software radio application, wireless LANs (WLANs), will be investigated using a simulation of a useful software radio modulation approach (OFDM) as well as potential software radio signal processing approaches that exploit antenna diversity. The utility of antenna diversity for WLANs has been demonstrated and the development and fielding of such systems is already under way, see [2] for examples. The consideration of OFDM and antenna diversity as parts of a limited software radio architecture assumes that the hardware resources are already in place. At this point it is useful to focus some attention on different processing schemes and their achievable performance.

The scenario considered in these simulations is a large 20 m × 10 m × 3 m room, which will reasonably have two transmitters for good coverage. The transmitting antennas are omnidirectional. The receive antennas are either omnidirectional or exhibit a realistic microstrip antenna beam response. The channel response is simulated using the stochastic image-based indoor channel (SIBIC) model [3]. This channel model treats equally elevation and azimuth angles while featuring deterministic and stochastic parameters.

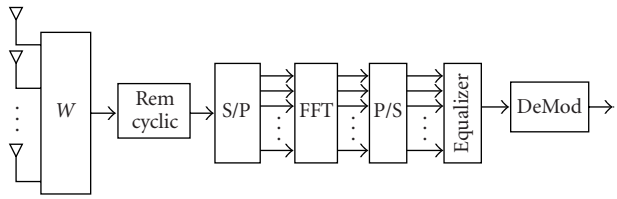

Figure 1: Block diagram of a baseband OFDM time domain receiver, adapted from [1] with addition of receiver array.

Other indoor channels listed for reference include [4, 5] and those listed in [6]. It is noted here that there is a concurrent work published in [7] for modeling the impulse response in time, but this model does not feature angles of arrival.

2. ORTHOGONAL FREQUENCY-DIVISION MULTIPLEXING SCHEME

OFDM is a modulation scheme that converts a frequency-selective channel into parallel flat fading channels by decreasing the symbol rate in each channel and that removes intersymbol interference by buffering the transmitted signal. As a result, OFDM simplifies channel equalization at the receiver. OFDM remains popular, although inherent problems such as interchannel interference, phase synchronization, and high peak-to-mean power makes achieving the ideal flat channel response difficult. Originally developed in the 1950s for military use, it is now found in applications such as digital terrestrial television broadcasting [8], and standards such as IEEE 802.11a and 802.11g WLAN. OFDM is also flexible in its modulation scheme, making it an ideal choice for limited software radio systems as well.

Since OFDM is an established modulation scheme, and references to it are accessible (examples include [9, 10, 11]), only a brief discussion of the receiver we use is provided. A block diagram of it is drawn in Figure 1.

The receiver used is a time-based receiver and has weights located directly after each antenna elements. In this configuration, the symbols are spread over time, requiring faster processors but fewer FFT circuits. Additionally, the cyclic prefix symbols are available and can be used to estimate the channel.

3. THE STOCHASTIC IMAGE-BASED INDOOR CHANNEL MODEL

In any receiving scheme with multiple antennas, such as a smart antenna array, the spatiotemporal correlation between the multipath components and each receiving element is of utmost importance. Simulations of receiver schemes using a channel model that produces incorrect spatiotemporal correlation will yield performance results that are unrealistic as the spatiotemporal correlation is a measure of the propagation scenario. For this reason, the SIBIC model (see [12, 13]) is the channel model of choice. The SIBIC model is a 3D, stochastic model that combines a deterministic foundation (the image method model) with statistical perturbations modeled after real measurements to simulate a desired propagating environment.

The starting point of the SIBIC model is the assumption of a rectangular room, a shape feature of most rooms. The image method is applied to find images of the transmitter, then these images are replaced with clusters whose rays have Poisson distributed arrivals, that is, exponentially distributed times-of-arrival (TOA); exponentially decaying amplitudes; and Laplacian distributed angle-of-arrival (AOA) with mean values determined by each image position. See Figure 2 for visual representation of the model, and Figure 3 for link between the time-of-arrival, angle-of-arrival, and corresponding amplitude. Finally, receiver effects such as limited bandwidth and noninteger sampling are added to the model via filtering with a window.

Several key components of the SIBIC model will now be discussed: the partition-dependent path loss model, the separable AOA distribution function, the Poisson intracluster arrival distribution function, and the intracluster ray amplitude function.

The partition-dependent path loss model is

$$P_L(d) = 10n\log_{10}\left(\frac{4\pi d}{\lambda_c}\right) + \sum_{i}^{W} X_i, \tag{1}$$

where n is the path loss exponent, d is the distance from the receiver to each virtual source, W is the total number of walls between the receiver and the virtual source, and X_i is the partition-dependent attenuation factor in dB.

The 3D channel impulse response is assumed separable, that is,

$$h(t,\theta,\phi) = h(t)h(\theta)h(\phi), \tag{2}$$

where $h(t)$ is the TOA function, $h(\theta)$ is the zenith AOA function, and $h(\phi)$ is the azimuth AOA function. This is an extension of the 2D separable channel of [13].

The extended 3D angular distribution with both angles is the product of two independent Laplacian functions denoted by the expression

$$p(\theta,\phi) = \frac{1}{\sqrt{2}\sigma}e^{-|\sqrt{2}\theta/\sigma|}\frac{1}{\sqrt{2}\sigma}e^{-|\sqrt{2}\phi/\sigma|}, \tag{3}$$

where σ denotes the angular standard deviation, θ denotes the azimuth angle, and ϕ denotes the elevation angle. Both θ and ϕ are relative to their cluster mean.

The perceived angular spread of the cluster source at the receiver decreases as the distance between the cluster and the receiver increases. This makes the angular spread a function of the described distance, which is depicted in Figure 4. At a distance d_1, the angular spread of a clustered source is σ_1, so for this relationship the angular spread is σ_2 at a distance d_2.

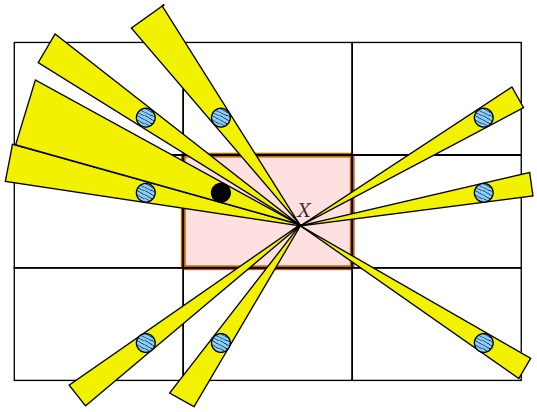

Figure 2: An overview of the proposed model. The "X" at the center of the beams represents the receiver, the solid and dashed circles represent the transmitter and its images, respectively. The highlighted room is the room of interest. The other surrounding rooms are some of the imaged rooms. The finite-width rays extending from the receiver are visualizations of the effect of introducing clusters.

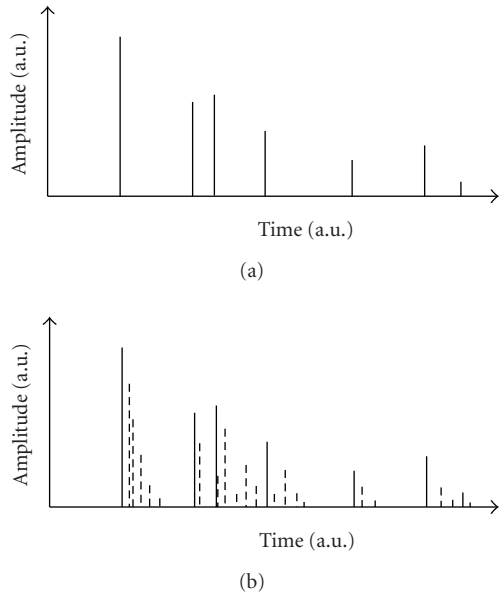

Figure 3: Visualization of an unfiltered impulse response for the image model and the SIBIC model. Notice that the first rays of each cluster are present in both models with the same amplitudes and time delays. However, the SIBIC model contains additional clusters, visually observed as the exponentially decreasing rays that follow the rays generated by the image model. (a) Image model. (b) Proposed model.

The equation that describes this relation is

$$\sigma_2 = \tan^{-1}\left(\frac{d_1 \tan(\sigma_1)}{d_2}\right). \tag{4}$$

In the simulations, a nominal angular spread at distance d_o and each distance d is used to calculate the angular spread of each cluster.

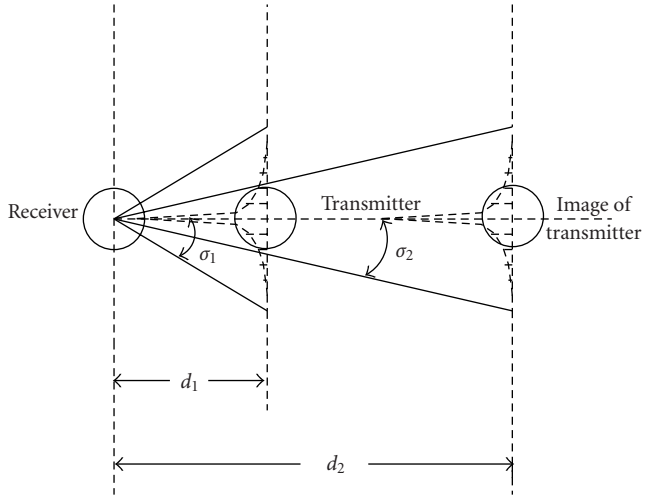

Figure 4: Angular spread of transmitter and its image as perceived by the receiver. The circles are visualizations of the receiver, the transmitter, and the image of the transmitter. Using basic geometry, the width of the angular spread is calculated using a spread and a distance reference value. In this case d_1 and σ_1 are the referenced values, d_2 is a known value, and σ_2 is the resulted calculated value.

As discussed, a Poisson process describes the arrivals of the rays within each cluster, with λ denoting the intracluster (rays within the cluster) rate, T_l the arrival time of the lth cluster, and $\beta(T_l)$ the amplitude of the lth cluster of the Poisson process. From T_l, d can be calculated, and then $\beta(T_l)$ via (1). The time of arrival t_{k+1} of the $(k+1)$st ray after the kth ray in any cluster is expressed by the conditional probability density function

$$p(t_{k+1} \mid t_k) = \lambda e^{-\lambda(t_{k+1}-t_k)}. \tag{5}$$

The amplitude of the $(k+1)$st ray in the cluster is expressed as

$$\beta(T_l, k+1) = \beta(T_l) e^{-(t_{k+1}-T_l)/\gamma}, \tag{6}$$

where γ is the exponential power delay constant of the cluster.

Simulation and measurement results of the channel are generally compared by examining parameters such as mean excess delay ($\bar{\tau}$), rms delay spread (σ_τ), or power delay profile shapes (PDP(τ_i)). These parameters are measures of the multipath channel response. The mean excess delay is defined as the first moment of the power delay profile relative to a power threshold (when $\tau = 0$). The expression for the mean excess delay of a sampled PDP is

$$\bar{\tau} = \frac{\sum_{\tau_i} \mathrm{PDP}(\tau_i)\tau_i}{\sum_{\tau_i} \mathrm{PDP}(\tau_i)}, \tag{7}$$

Table 1: Parameters used in OFDM simulations.

Room Size (m)	$20 \times 10 \times 3$
SNR (dB)	10
Carrier frequency (GHz)	60.0
Receiver antenna	Omni and microstrip
Transmitter antenna	Omni
Receiver position (m) (x, y, z)	(varies,varies,1)
Transmitter position (m) (x, y, z)	$(5, 5, 2.9)$ and $(15, 5, 2.9)$
Maximum number of reflections	3
Maximum time response (ns)	200
Exponential parameter (γ) (ns)	9.0
Poisson parameter $(1/\lambda)$ (ns)	5.0
Angular spread of at 5.0 m	20.0°
Receiver bandwidth (MHz)	100
Sampling frequency (GHz)	1.0
Hanning window time width (ns)	20.0
Path loss exponent (n)	2
Partition loss factor (X) (dB)	5

where τ_i denotes the sampling time of the power delay profile. The rms delay spread is the square root of the second moment of the power delay profile. The expression for the rms delay spread is

$$\sigma_\tau = \sqrt{\overline{\tau^2} - (\bar{\tau})^2}, \tag{8}$$

where

$$\overline{\tau^2} = \frac{\sum_{\tau_i} \mathrm{PDP}(\tau_i)\tau_i^2}{\sum_{\tau_i} \mathrm{PDP}(\tau_i)}. \tag{9}$$

Variations between simulated and theoretical values of the mean excess delay and rms delay spread exist because of the power threshold. In simulating the channel response, a threshold time is used rather than a threshold power to signify when $\tau = 0$. The threshold time is set to the first incoming ray and is known. The parameters for simulating the channel are listed in Table 1. Also listed in this table is the SNR parameter that will be used later in the OFDM simulations.

Figures 5 and 6 are plots of the simulated mean excess delay and delay spread for the $20 \times 10 \times 3$ room. An omnidirectional and a microstrip antenna were used in simulating the values in each figure. The results indicate that the mean excess delay is largest near the transmitters and smallest away from transmitters. On the other hand, the trend is reversed with the delay spread. Additionally, symmetry occurred in both of these simulated values around the transmitters. According to [2], the expected values of the mean excess delay and delay spread are in the nanosecond range for an indoor environment. It is noted here that to compare simulated to measured values is difficult as the instrument, threshold level, and propagating environment are almost always unique to each scenario.

4. OFDM SIMULATIONS WITH THE SIBIC MODEL

In the following discussion, the downlink performance of a single user in a large room is simulated for these receiver configuration: a single antenna receiver, a 4×4 planar fixed beamformer, and a 4×4 planar adaptive beamformer. The OFDM modulation is either QPSK or 16-QAM. In addition, the performance of QPSK with receivers having realistic beam patterns is also estimated via simulations. Receiver performance in small cells is important because access to base units from WLAN portable systems are from users who are generally indoor and stationary [2]. In the simulated $20\,\mathrm{m} \times 10\,\mathrm{m} \times 3\,\mathrm{m}$ room, two base units are placed near the ceiling and separated 10 m apart to provide good coverage. The basic setup is drawn in Figure 7, and the important simulation parameters are listed in Table 1.

At the transmitter, a 32-subcarrier FFT and a channel spacing of 3.125 MHz for a total receiver bandwidth of 100 MHz are used. After the FFT, a 10-sample cyclic prefix is added for a total extended time OFDM symbol sequence that is 42 samples long. The baseband sampling rate is 1 GHz. Additionally, a raised cosine window with a rolloff factor of 0.2 is used. The SNR is defined as bit energy over noise energy ($\mathrm{E}_b/\mathrm{N}_0$).

The receiving scheme of a single antenna is apparent and will not be discussed. With a fixed beamformer, the angle-of-arrival of the line-of-sight (LOS) ray is assumed known, so a beam at that angle is formed. A beam is formed with an adaptive beamformer using the optimal Wiener coefficients calculated from 50 OFDM symbols. Discussion of the adaptive scheme can be found in [14]. In both array methods, the spacing between antenna elements is half the carrier wavelength, that is, $d = 0.5\,\lambda_c$. In each receiving scheme, a 1-tap filter adapted at a step size of 0.005 based on the mean-squared criterion is used for equalization at every 6th subcarrier. The equalization coefficient of other subcarriers is achieved using linear interpolation of the in-phase and quadrature components.

The average mean-squared error (MSE) is used as a performance measure for each receiving scheme. It is calculated by averaging the MSE of the detected and transmitted frequency symbols across 32 subcarriers and over 500 symbols at each position within the room. At each position, 1000 OFDM symbols (1050 for the adaptive beamformer) are transmitted. With the single-element receiver and fixed beamformer, the first 500 symbols are for adapting the equalizer and the last 500 symbols are for calculating the MSE. With the adaptive beamformer, 50 additional symbols are transmitted beforehand for estimating the Wiener filter coefficients. It is noted here that 500 symbols for adapting the equalizer is a generous value, but it allows for a small step size and assured stability of the equalizer to reach a steady-state MSE at most positions within the room.

For the channel model, the response is assumed to be the *cluster LOS* case of the SIBIC model, narrowband, and normalized to a referenced channel power. Specifics of the *cluster LOS* case are discussed in [3, 12]. Since the bandwidth to carrier frequency ratio is substantially less than one percent,

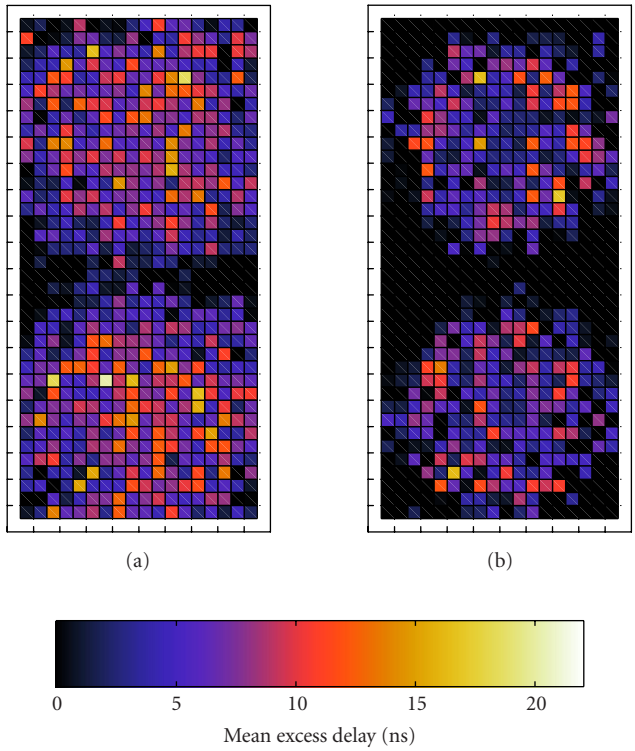

Figure 5: Simulated mean excess delay of channel using parameters in Table 1. (a) Omnidirectional. (b) w/ beam pattern.

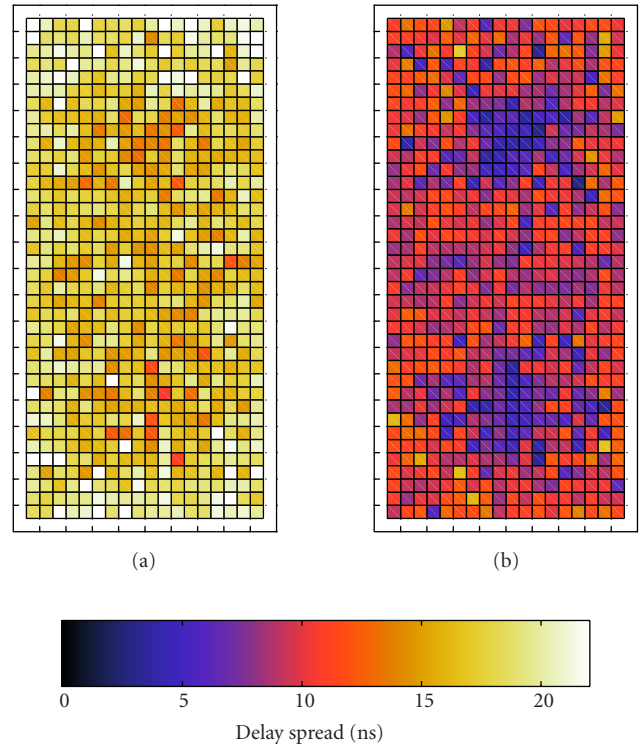

Figure 6: Simulated delay spread of channel using parameters in Table 1. (a) Omnidirectional. (b) w/ beam pattern.

the narrowband assumption is safe. The channel is normalized at one antenna element so that the SNR can be easily defined for the simulations. Additionally, the same channel is used in each receiving scheme in all following subsections and the channel is assumed time constant at each position.

4.1. QPSK

The MSE of the three receiving schemes with QPSK modulation and omnidirectional antennas are plotted in Figure 8. Recall the base units are located at $(5, 5, 2.9)$ and $(15, 5, 2.9)$. Visually, the single-element receiver has the poorest performance, the fixed beamformer is better, and the adaptive beamformer is best. There is an observable difference of at least 5 dB centered around the positions of both base units, with the best performance achieved using the adaptive beamformer. For an arbitrary MSE value of -10 dB, the fraction of positions with MSE below this value is 1, 47, and 99 percent for the single element, fixed beamformer, and adaptive beamformer, respectively.

Since the single element receiver has equal gain toward all angles, the fixed beamformer has highest gain in the LOS angle, and the adaptive beamformer uses the approximate Wiener solution, the improvement trend from single element to adaptive beamformer is reasonable. Moreover, it is expected that the SNR of the fixed beamformer in the LOS angle increases by the number of antenna elements. For the adaptive beamformer, analysis of the resultant beam pattern (not plotted) shows that the mainlobe in the simulations

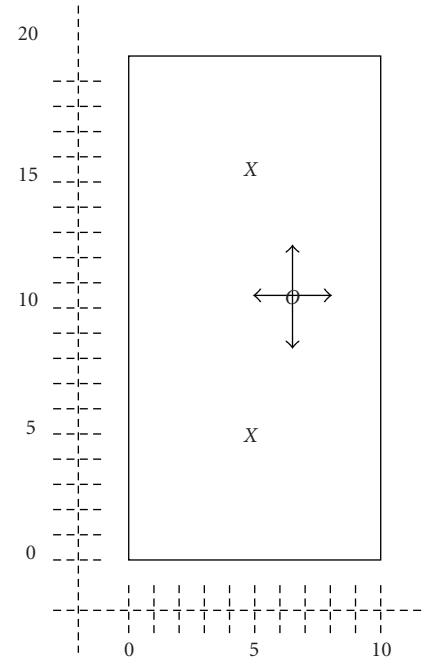

Figure 7: General simulation scenario. The two "X's" represent the two base units. The "O" represents the mobile unit, which is positioned at various locations in the room. The dimension of the room is $20 \times 10 \times 3\ \text{m}^3$. The base units are located at a height of 2.9 m. The mobile unit is located at a height of 1.0 m. The mobile unit consists of a single element, a 4×4 planar array using a LOS fixed beamformer, and a 4×4 planar array using an adaptive beamformer.

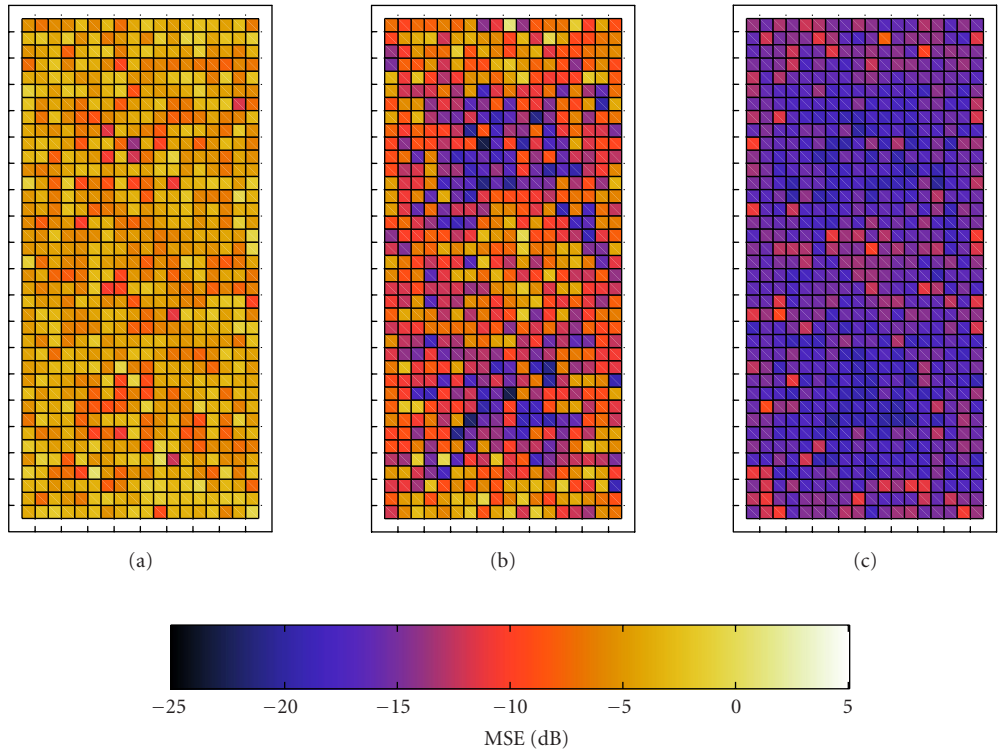

Figure 8: Average MSE of 32 subcarriers, averaged over 500 OFDM symbols, with 4-QAM modulation. (a) 1 element M = 6. (b) Fixed beamformer M = 6. (c) Adaptive beamformer M = 6.

was directed at the LOS ray and nulls were place towards strong multipath rays. This angular response pattern is sensible since multipath signals distort the signal from the LOS ray, which is the signal of interest. In addition, the lowest MSE values are obtained near the base units where the spread of the channel is at a minimum. It is also noted here that since the wavelength at 60 GHz is only 5 mm, the channel is significantly different between sampled positions. This is a possible reason why high and low MSE squares are occasionally next to each other.

4.2. 16-QAM

With omnidirectional antennas, the MSE of the three receiving schemes are simulated again, but this time with 16-QAM. The results are plotted in Figure 9. As was noted, the SNR is kept constant by reducing the noise power by $\sqrt{2}$ from QPSK to maintain the same bit-energy-to-noise-power ratio. The improvement in MSE from 4-QAM to 16-QAM is 0.2, 0.2, and 1.2 dB for single element, fixed beamformer, and adaptive beamformer, respectively. It is noted here that this improvement in MSE does not directly correspond to better performance since signal constellations with different densities are being compared.

4.3. QPSK with beam pattern

In an outdoor environment, the base and mobile units are widely separated. As a result, modeling the receiving antennas as omnidirectional is justified since the multipath signals are mostly from angles near the horizon and the angular response for a vertical dipole is uniform in azimuth. However, the mobile and base units in an indoor environment are near each other and the elevation angle can no longer be assumed to be from near the horizon. Therefore, the system performance is dramatically affected by the angular response of the antennas, particularly at the null angles of the antennas. It is beneficial then to simulate the angular response for a realistic pattern rather than with an assumed omnidirectional pattern to investigate the performance of a receiver that is located indoor.

In this subsection, the receiver performance with QPSK modulation is simulated using antenna elements having angular responses modeled after a realistic microstrip antenna pattern measured in [15]. The duplicated pattern is plotted in Figure 10. Differences between the duplicated and original pattern are twofold. First, the gain of the duplicated pattern is several dB higher at elevation angles greater than 60 degrees from vertical. Second, the duplicated pattern is normalized to the gain at the vertical angle, whereas the original pattern is not normalized.

The results of these simulations are plotted in Figure 11. There is an overall mean of 2.2, 2.2, and 0.7 dB MSE improvements compared to QPSK with omnidirectional antennas for the single-element receiver, fixed beamformer, and adaptive beamformer, respectively. In the same order,

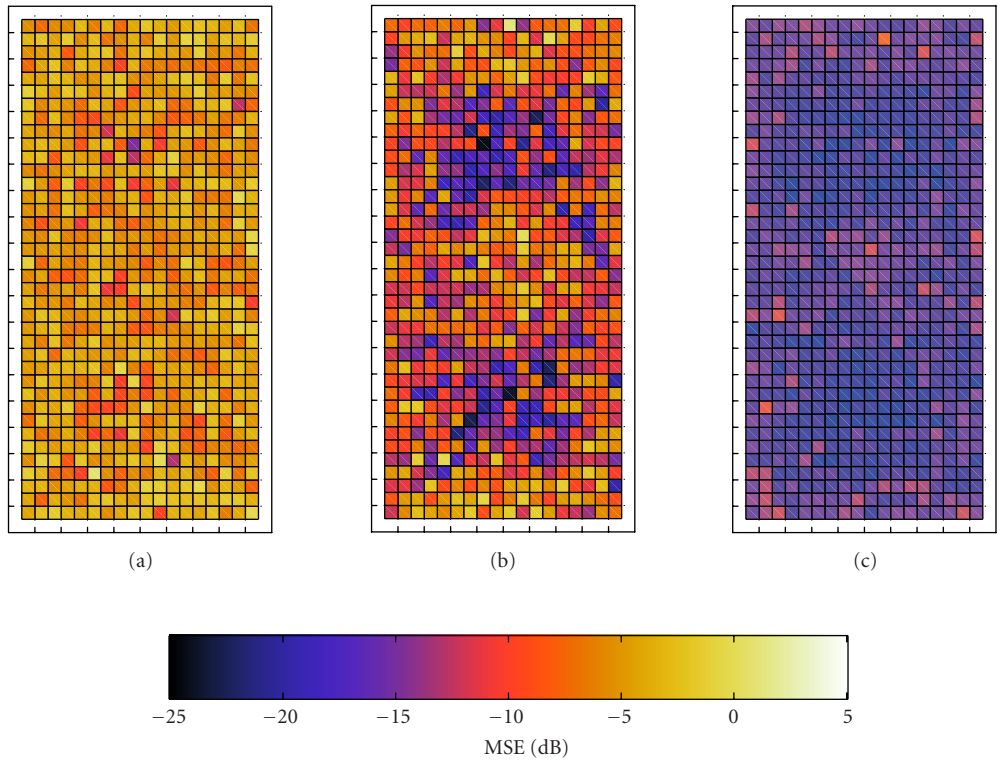

Figure 9: Average MSE of 32 subcarriers, averaged over 500 OFDM symbols, with 16-QAM modulation. (a) 1 element M = 6. (b) Fixed beamformer M = 6. (c) Adaptive beamformer M = 6.

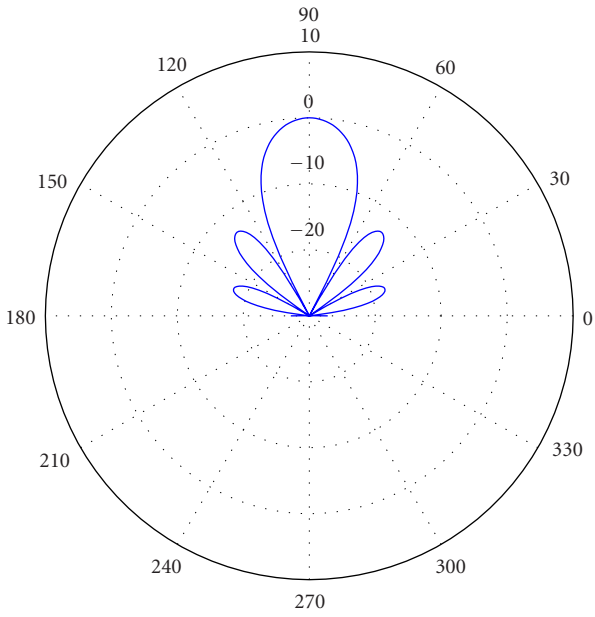

Figure 10: Radiation pattern response for microstrip antennas at 60 GHz, adapted from [15] with a sinc function of order 2.

the number of positions with better performance is 81, 73, and 68 percent. Overall, this means that simpler receiving schemes improve more compared to sophisticated receiving schemes with directive antennas. In addition, it is noticed that most improvement occurs at positions where the angles of the mobile unit may be in the center of either the main or sidelobes of the antenna beam pattern, and most degradation occurs at positions where the mobile units are at the nulls of the antenna beam pattern.

5. CONCLUSION

The performance of three software radio antenna diversity schemes (a single antenna, a 4×4 fixed-beamformer planar array, and a 4×4 adaptive-beamformer planar array) was investigated via the SIBIC channel model using candidate software radio OFDM modulation schemes, including QPSK and 16-QAM. The results clearly indicate that the more sophisticated receiver schemes outperform simpler schemes by decreasing the mean MSE and extending coverage. This indicates a software radio WLAN would be capable of enhancing performance by switching to more DSP intensive approaches. In addition, the authors would recommend the use of the full 3D SIBIC channel model for future investigations of software defined processing for indoor WLANs that exploit antenna diversity.

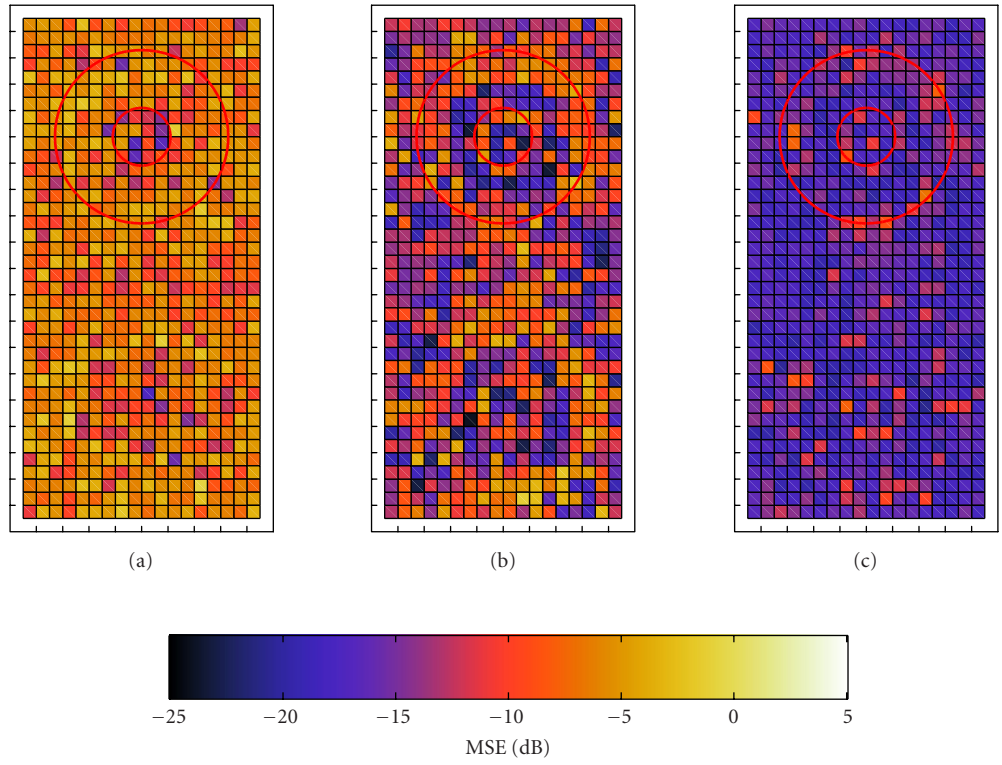

Figure 11: Average MSE of 32 subcarriers, averaged over 500 OFDM symbols, with 4-QAM modulation. A microstrip antenna pattern was applied, as compared to previous simulation cases using omnidirectional antennas. The small (5 pixels wide) circle corresponds to the base unit being at 60 degrees, while the large (13 pixels wide) circle corresponds to the base unit being at 30 degrees, in elevation with respect to the mobile unit. (a) 1 element M = 6. (b) Fixed beamformer M = 6. (c) Adaptive beamformer M = 6.

REFERENCES

[1] T. Keller and L. Hanzo, "Adaptive multicarrier modulation: a convenient framework for time-frequency processing in wireless communications," *Proc. IEEE*, vol. 88, no. 5, pp. 611–640, 2000.

[2] T. S. Rappaport, A. Annamalai, R. M. Buehrer, and W. H. Tranter, "Wireless communications: past events and a future perspective," *IEEE Commun. Mag.*, vol. 40, no. 5, pp. 148–161, 2002.

[3] K. D. Le, M. W. Hoffman, and R. D. Palmer, "Three-dimensional propagation model for wireless LAN distribution of software radio," in *Proc. IEE Colloquium on DSP Enabled Radio*, Livingston, Scotland, UK, September 2003.

[4] R. Heddergott and P. E. Leuthold, "An extension of stochastic radio channel modeling considering propagation environments with clustered multipath components," *IEEE Trans. Antennas Propagat.*, vol. 51, no. 8, pp. 1729–1739, 2003.

[5] C.-C. Chong, C.-M. Tan, D. I. Laurenson, S. McLaughlin, M. A. Beach, and A. R. Nix, "A new statistical wideband spatio-temporal channel model for 5-GHz band WLAN systems," *IEEE J. Select. Areas Commun.*, vol. 21, no. 2, pp. 139–150, 2003.

[6] R. B. Ertel, P. Cardieri, K. W. Sowerby, T. S. Rappaport, and J. H. Reed, "Overview of spatial channel models for antenna array communication systems," *IEEE Pers. Commun.*, vol. 5, no. 1, pp. 10–22, 1998.

[7] J. Kunisch and J. Pamp, "An ultra-wideband space-variant multipath indoor radio channel model," in *Proc. IEEE Conference on Ultra Wideband Systems and Technologies (UWBST '03)*, vol. 1, pp. 290–294, Reston, Va, USA, November 2003.

[8] H. Sari, G. Karam, and I. Jeanclaude, "Transmission techniques for digital terrestrial TV broadcasting," *IEEE Commun. Mag.*, vol. 33, no. 2, pp. 100–109, 1995.

[9] R. Van Nee and R. Prasad, *OFDM for Wireless Multimedia Communications*, Artech House, Boston, Mass, USA, 2000.

[10] L. Hanzo, M. Münster, B. J. Choi, and T. Keller, *OFDM and MC-CDMA for Broadband Multi-User Communications, WLANs and Broadcasting*, John Wiley & Sons, Chinchester, UK, 2003.

[11] J. Heiskala and J. Terry, *OFDM Wireless LANs: A Theoretical and Practical Guide*, SAMS, Indiana, USA, 2002.

[12] K. D. Le, M. W. Hoffman, and R. D. Palmer, "A stochastic image-based indoor channel model for use in ultra-wideband 3-D sensor array simulations," in *Proc. IEEE Conference on Ultra Wideband Systems and Technologies (UWBST '03)*, vol. 1, pp. 300–304, Reston, Va, USA, November 2003.

[13] Q. H. Spencer, B. D. Jeffs, M. A. Jensen, and A. L. Swindlehurst, "Modeling the statistical time and angle of arrival characteristics of an indoor multipath channel," *IEEE J. Select. Areas Commun.*, vol. 18, no. 3, pp. 347–360, 2000.

[14] B. Farhang-Boroujeny, *Adaptive Filters: Theory and Applications*, John Wiley & Sons, Chinchester, UK, 1998.

[15] M. A. Weiss, "Microstrip antennas for millimeter waves," *IEEE Trans. Antennas Propagat.*, vol. 29, no. 1, pp. 171–174, 1981.

Khoi D. Le received the B.S. and M.S. degrees in electrical engineering from the University of Nebraska at Lincoln in 1999 and 2001, respectively. Currently, he is working towards the Ph.D. degree at the University of Oklahoma, where he is conducting research in the signal processing of remotely sensed data of atmospheric scatterers with radars. His interests include wireless communications, adaptive filtering techniques, and stratiform clouds.

Michael W. Hoffman received the B.S. degree from Rice University, Houston, Texas, the M.S. degree from the University of Southern California, Los Angeles, and the Ph.D. degree from the University of Minnesota, all in electrical engineering. From 1985 to 1988, he was a signal processing system engineer in the Space Communications Division of TRW Inc. In 1993, he joined the University of Nebraska-Lincoln, where he currently serves as an Associate Professor. His research interests include data compression, joint source-channel coding, and sensor array processing.

Robert D. Palmer received his Ph.D. degree in electrical engineering from the University of Oklahoma, Norman, Oklahoma, in 1989. His Ph.D. studies focused on the applications of advanced signal processing techniques to atmospheric radar. From 1989 to 1991, he was a Postdoctoral Fellow at the Radio Atmospheric Science Center, Kyoto University, Japan. After his stay in Japan, Professor Palmer held the position of a Research Associate in the Physics Department, Clemson University, South Carolina. From 1993 to 2004, he was a member of the faculty of the Department of Electrical Engineering, the University of Nebraska-Lincoln, where his interests broadened into areas including wireless communications, remote sensing, and pedagogy. He joined the faculty of the School of Meteorology, the University of Oklahoma (OU) in 2004, where he holds the rank of a Professor. He is also an Adjunct Professor in the School of Electrical and Computer Engineering at OU. He has published extensively in the general area of radar remote sensing of the atmosphere, with emphasis on the use of multiple frequencies/receivers for interferometry and generalized imaging problems.